International Core Journal of Engineering Volume 11 Issue 6, 2025
ISSN: 2414-1895 DOI: 10.6919/ICJE.202506_11(6).0041

Design and Performance Analysis of a Jet Self-Priming Microbubble Generator with Annular Air Orifices based on CFD-PBM

Guoqing Li[a], Juan Zhao[*], Jiawei Mou, Ruiyan Yu, Weijun Gao, Jinming Jiang

Qingdao University of Technology, Qingdao 266525, China

[a]1244965549@qq.com

Abstract

Microbubble generators are widely used in industrial production, but single-sided air intake can induce bubble eccentricity and uneven size distribution, limiting their performance. To address this issue, a BH-type jet self-priming microbubble generator was proposed, featuring annular air orifices, arc-shaped flow channels, and a stepped tube structure. Visualization experiments were conducted to obtain key simulation parameters, and a CFD-PBM coupled model incorporating the Luo breakup-coalescence mechanism was established to systematically analyze the effects of structural parameters on bubble size distribution. Simulation results show that annular air orifices prevent bubble eccentricity, arc-shaped flow channels reduce the formation of large bubbles, and bubble size remains stable in the stepped tube (0.63±0.12 mm). The optimal configuration was found to be six air orifices and a 3.5° diffuser angle, achieving a gas-liquid mixing uniformity of 45% and an average bubble size of 730 μm. This study demonstrates that the BH-type microbubble generator effectively reduces bubble size and enhances gas-liquid mixing, providing a scalable solution for flotation separation and chemical reactor optimization.

Keywords

CFD-PBM; Microbubble Generator; Structural Design; Gas-Liquid Two-Phase Flow.

1. Introduction

Microbubble generators have been widely applied in various fields such as mineral flotation [1,2], water treatment [3,4], and chemical engineering [5], owing to their simple structure, strong adaptability, and ability to produce suitable microbubbles. However, they still face challenges such as limited air intake, uneven bubble size distribution, eccentric bubble aggregation, and insufficient gas–liquid mixing [6–8]. To tackle these issues, researchers often combine visualization experiments with numerical simulations to explore internal flow characteristics and bubble breakup mechanisms, achieving considerable progress in recent years.

Bie et al. [9] and Tang et al. [10] used high-speed cameras to capture the motion and deformation of bubbles. Their experiments revealed that bubbles are broken into smaller ones due to turbulent shear after entering the diffuser pipe. Xu et al. [11] proposed that an increase in pressure drop promotes bubble breakup, identifying it as a key influencing factor. Xu et al. [12] incorporated the Luo model into the population balance model (PBM), using the bins method to classify bubble groups of different sizes. The simulation results, verified by visualization experiments, effectively described the processes of bubble breakup and coalescence. Liu et al. [7] examined the influence of air intake structures on bubble dynamics. Their findings showed that a single-side intake induces eccentric bubble motion, where the region of higher gas holdup is opposite the intake pipe, affecting the

ISSN: 2414-1895 DOI: 10.6919/ICJE.202506_11(6).0041

distribution of bubble sizes. In practical applications, such eccentric motion accelerates pipe wall wear on one side, shortening equipment lifespan. Furthermore, it reduces bubble velocity, which promotes aggregation and coalescence, leading to larger bubble sizes. To improve bubble behavior, Cao et al. [13] and Ding et al. [14] studied the effects of intake pipe positioning on bubble trajectories. Their research indicated that the initial bubble shape significantly affects bubble size. Although repositioning the intake pipe can alleviate bubble aggregation to some extent, it cannot eliminate the eccentric effect caused by a single intake. Therefore, preventing eccentric bubble motion induced by single-side air inlets, enhancing gas–liquid mixing, and optimizing bubble size distribution remain critical challenges.

Therefore, this study proposes a novel jet-type microbubble generator (BH-type) to address the limitations of single-side intake pipe structures. A visualization experimental platform was constructed to obtain simulation parameters, and the effects of structural parameters on the internal flow characteristics and bubble size were investigated using a CFD–PBM coupled model.

2. Determination of Key Parameters for the BH-Type Microbubble Generator

2.1 Structural Design and Experimental Platform of the BH-Type Microbubble Generator

The BH-type microbubble generator consists of six key structural components: a converging tube, annular air orifice, arc-shaped flow channel, air intake chamber, stepped tube, and diffuser pipe, as illustrated in Figure 1. This structural design aims to optimize microbubble generation characteristics, mitigate the bubble eccentricity caused by a single intake pipe, and improve the uniformity of bubble size distribution.

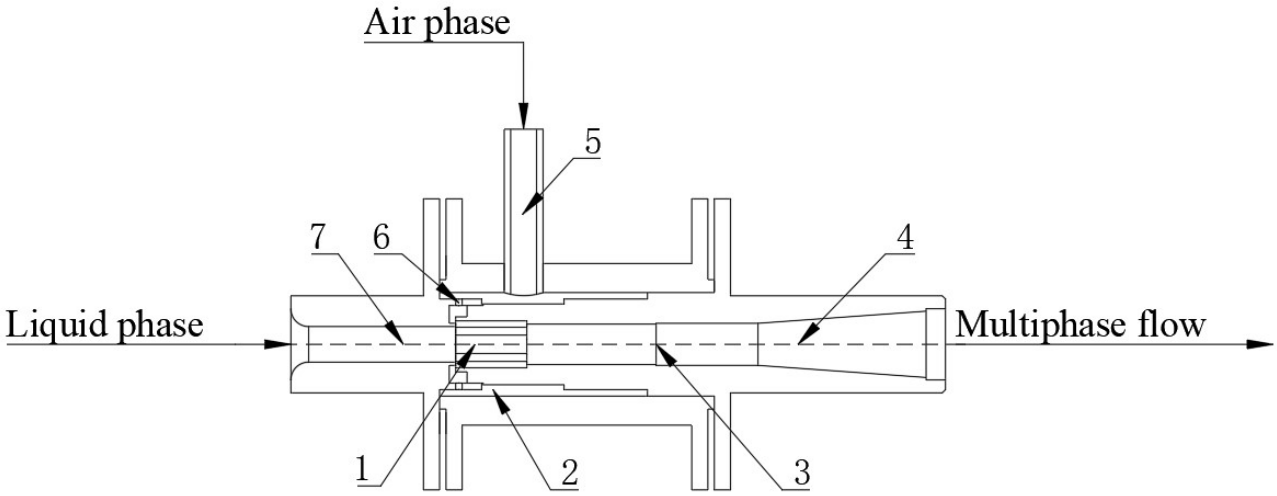

Figure 1. Schematic diagram of microbubble generator structure

(1. Arc-shaped Flow Channel, 2. Air Intake Chamber, 3. Stepped Tube, 4. Diffuser Pipe, 5. Intake Pipe, 6. Annular Air Orifice, 7. Converging Tube)

To measure experimental data such as gas–liquid flow rates and pressure values of the BH-type microbubble generator, a custom simulation parameter acquisition system was designed and constructed. The procedure is illustrated in Figure 2 [15,16]. By adjusting the frequency of the centrifugal pump motor, the liquid flow rate was controlled to match actual working conditions, and instrument data were recorded every 2 minutes. Meanwhile, a high-speed camera was used to capture bubble images inside the observation chamber, and Python was employed for image processing and data extraction.

ISSN: 2414-1895 DOI: 10.6919/ICJE.202506_11(6).0041

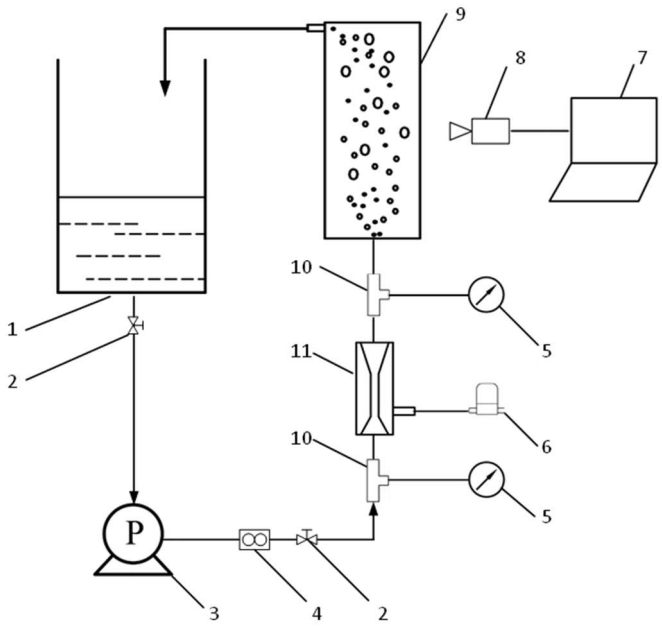

Figure 2. Microbubble generator performance evaluation device
(1. water storage tank, 2. water valve, 3. centrifugal pump, 4. liquid flow meter, 5. pressure gauge, 6. gas flow meter, 7. laptop computer, 8. high-speed camera, 9. bubble observation chamber, 10.tee pipe, 11. microbubble generator)

Based on the captured black-and-white bubble images, Gaussian filtering was first applied to suppress image noise. A fixed threshold segmentation method was then used to extract bubble regions. Subsequently, connected domain analysis was performed to calculate the contour pixel area, which was converted into equivalent diameters using a calibrated scale. Finally, a histogram of the bubble size distribution was generated. This method was implemented using the OpenCV library, achieving an extraction error of less than 5%, which meets the statistical accuracy requirements.

2.2 Experimental Results and Simulation Parameter Extraction

The clean water experimental data are shown in Table 1. The liquid flow rate and outlet pressure were selected as the boundary conditions for the numerical simulation, with the inlet pressure used as the validation condition. Meanwhile, the processed images were used to obtain the bubble size distribution, as shown in Figure 3. The average bubble diameter was 1075 μm, which was taken as the initial bubble size.

Table 1. Microbubble generator water experiment data

Serial Number	Liquid flow L/min	Gas flow L/min	Entry pressure /kPa	Exit pressure /kPa
1	63.42	16.55	67.2	18.1
2	64.15	15.36	65.5	19.2
3	62.43	17.67	67.9	17.3
4	63.86	16.57	66.9	18.0
5	63.52	16.86	67.3	17.9

ISSN: 2414-1895 DOI: 10.6919/ICJE.202506_11(6).0041

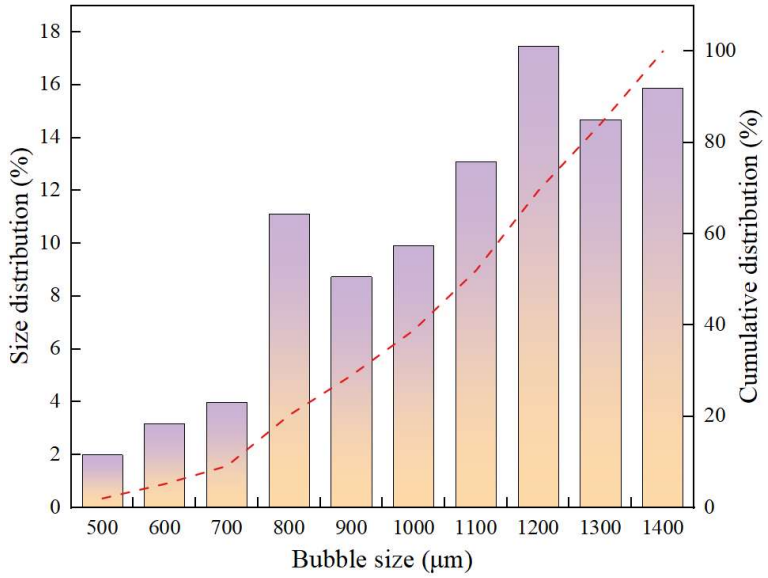

Figure 3. Bubble size distribution

3. Establishment of the Numerical Simulation Model and Boundary Conditions

3.1 Creation of the Computational Domain and Grid Generation for the BH-Type Microbubble Generator

In this study, the physical model of the BH-type microbubble generator was constructed using SolidWorks, and the mesh generation was performed in Ansys software through the Meshing module. A boundary layer was set in the near-wall region, and both structured and unstructured meshes were combined to effectively control the mesh quantity while ensuring mesh quality. The meshing results are shown in Figure 4.

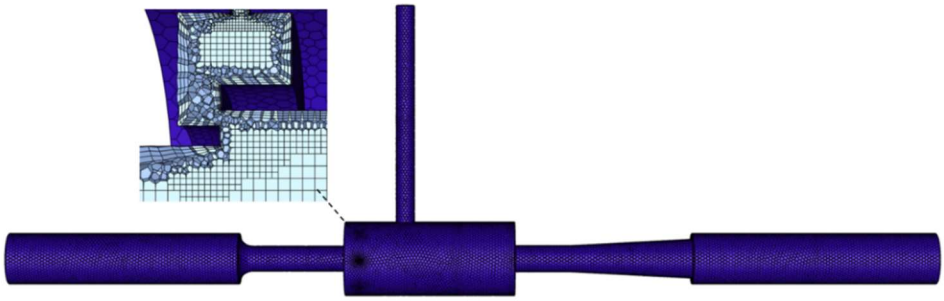

Figure 4. Fluid domain meshing

3.2 PBM Population Balance Model

To comprehensively analyze the bubble size distribution within the microbubble generator, the PBM model needs to be coupled, and the Luo breakup-Luo coalescence equations are introduced to investigate the bubble evolution process. The PBM model is combined with the bubble data obtained from the visualization experiments to classify different bubble groups, as detailed in Table 2.

Table 2. Sizes of the bubble bins.

Bin number	Mean bubble diameter, μm
Bin-0	970
Bin-1	584
Bin-2	351

ISSN: 2414-1895 DOI: 10.6919/ICJE.202506_11(6).0041

Table 2. Continued

Bin number	Mean bubble diameter, μm
Bin-3	211
Bin-4	127
Bin-5	76
Bin-6	46
Bin-7	28
Bin-8	17
Bin-9	10

3.3 Boundary Conditions and Solution Method

The liquid phase uses a velocity inlet with a velocity of 2.783 m/s. The gas phase uses a pressure inlet, with the pressure set to standard atmospheric pressure and the gas volume fraction set to 1. The mixture phase uses a pressure outlet with a pressure of 18.1 kPa. The primary phase of the multiphase flow is liquid water, and the secondary phase is air. The solution scheme adopts the Phase-Coupled SIMPLE algorithm for pressure-velocity coupling, with the pressure discretization scheme set to the PRESTO! algorithm. The relaxation factors are set to default values.

3.4 Grid Independence Verification

The mesh size was adjusted, and five sets of high-quality meshes were generated for grid independence verification. The inlet pressure of the converging tube was taken as the characteristic parameter, and the results are shown in Table 3. The results indicate that when the mesh number reaches 300,000, the pressure stabilizes, and the difference between two adjacent data sets is less than 1%. At this point, further increasing the mesh number has negligible effects on the simulation results. Considering factors such as computational accuracy and cost, a mesh number of 400,000 was selected for this study.

Table 3. Grid independence results

Number of grids/$\times 10^4$	Simulation result /kPa	Experimental result /kPa	Relative error/%
20	76.37	67.16	13.98
30	69.72	67.16	4.06
40	69.26	67.16	3.37
50	69.86	67.16	4.27
60	69.52	67.16	3.77

4. Numerical Simulation Results and Analysis

4.1 Internal Flow Characteristics of the Microbubble Generator

The numerical simulation results show that the gas–liquid mixing process inside the microbubble generator is influenced by both the flow field structure and local flow conditions. As the liquid flows through the converging tube, its velocity rapidly increases from 3 m/s to 13 m/s, forming a stable high-speed jet. According to Bernoulli's principle, the pressure inside the arc-shaped flow channel drops to -15 kPa, causing the gas to be drawn into the tube through the annular air orifice. In the initial stage, as shown in Figure (b), the gas phase has a relatively low velocity and is primarily distributed in the arc-shaped flow channel. However, under the strong shear action of the high-speed liquid, the bubbles are quickly broken and dispersed to the central region, achieving preliminary mixing. When the gas–liquid two-phase flow enters the stepped tube, the fluid velocity reaches 13 m/s again due to the reduction in tube diameter, and the velocity difference between the central region and the near-

ISSN: 2414-1895 DOI: 10.6919/ICJE.202506_11(6).0041

wall region decreases. From Figure 6, it can be observed that the gas phase distribution gradually becomes more uniform during this process. This indicates that high flow velocities can suppress the effects of viscous resistance, reduce the radial velocity difference, and improve the gas–liquid mixing degree. Finally, the cross-sectional area of the diffuser pipe rapidly increases, causing a velocity difference of 6 m/s between the central region and the near-wall region, forming a significant velocity gradient radially. At this point, the local viscous effects are enhanced, making the bubbles more prone to vortex formation and coalescence. At the same time, Figure (c) shows that the pressure drop inside the diffuser pipe reaches 38 kPa. The significant pressure gradient further promotes the breakage of the bubbles into smaller bubbles, thereby improving the gas–liquid mixing uniformity.

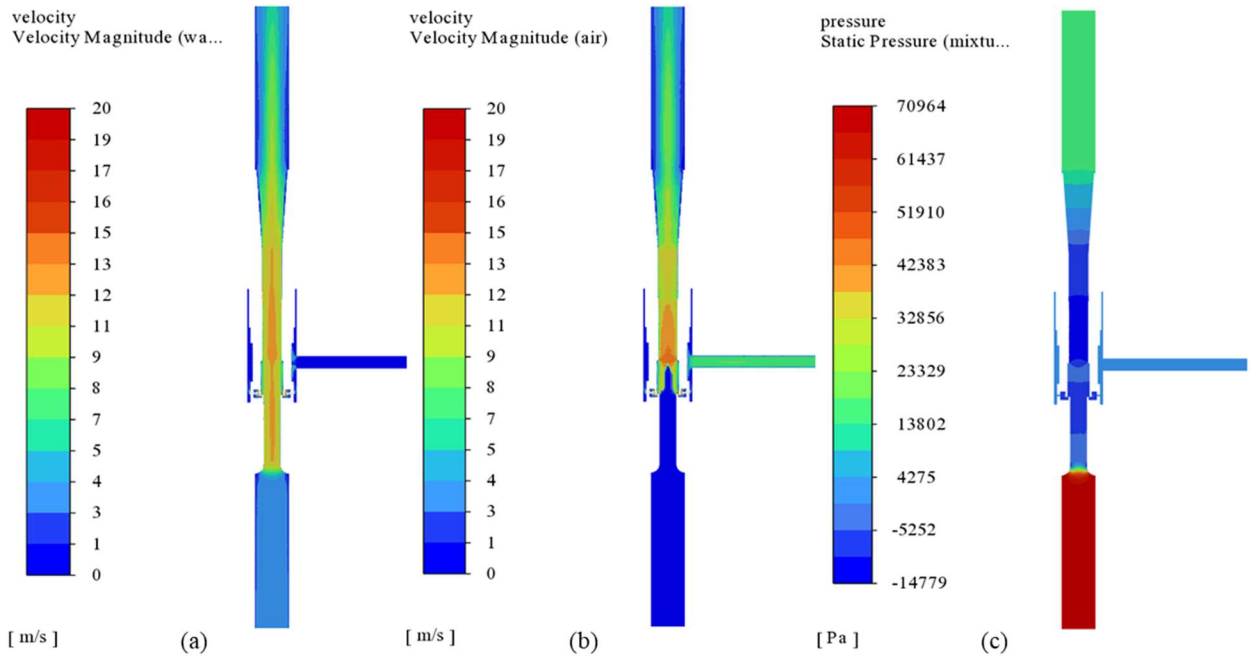

Figure 5. Internal flow field characteristics of the microbubble generator:
(a) Liquid phase velocity contour; (b) Gas phase velocity contour; (c) Pressure contour

4.2 Phase Distribution in the Microbubble Generator

As shown in Figure 6, due to the effect of the annular air orifice, the gas is evenly distributed in the arc-shaped flow channel, preventing the bubble eccentricity caused by the single intake pipe, thus providing favorable conditions for subsequent gas–liquid mixing. In the front section of the arc-shaped flow channel, the gas does not mix with the liquid, and the gas volume fraction is approximately 100%. In the latter section, the gas–liquid phases collide with the end face of the stepped tube, causing a backflow phenomenon. The gas volume fraction in the channel decreases to 80%, and the gas phase gradually migrates toward the central region. In the stepped tube region, due to the reduced tube diameter and the higher flow velocity in the central region, some of the gas remains concentrated near the tube wall. As the tube diameter gradually increases, the mixing effect improves, and the gas volume fraction near the wall is approximately 50%. In the diffuser pipe, due to the sharp increase in tube diameter, the pressure gradient is significantly enhanced, promoting the breakage of bubbles into smaller ones. At this point, the gas volume fraction reaches 45%, and the mixing effect is at its best. In the extension pipe, the gas volume fraction slightly decreases to 40%, but the overall mixing remains relatively uniform. This indicates that the pressure gradient in the diffuser pipe is the key factor in promoting bubble breakage and enhancing gas–liquid mixing.

By analyzing the gas-phase distribution near the wall of the stepped tube and diffuser pipe, as shown in Figure 5, it can be observed that when the flow velocity is low, viscous resistance tends to dominate, resulting in a reduced gas–liquid mixing degree at the wall. In contrast, in the stepped tube, where the flow velocity is higher, the effect of viscous resistance is suppressed, thereby improving the gas–

ISSN: 2414-1895 DOI: 10.6919/ICJE.202506_11(6).0041

liquid mixing effect. This indicates that viscous resistance plays a significant role in regulating gas-phase distribution, and its influence is dependent on the local flow velocity: when the velocity is too low, viscous resistance dominates, leading to worsened mixing, while increasing the velocity can effectively reduce the impact of viscous resistance and improve the gas–liquid mixing state.

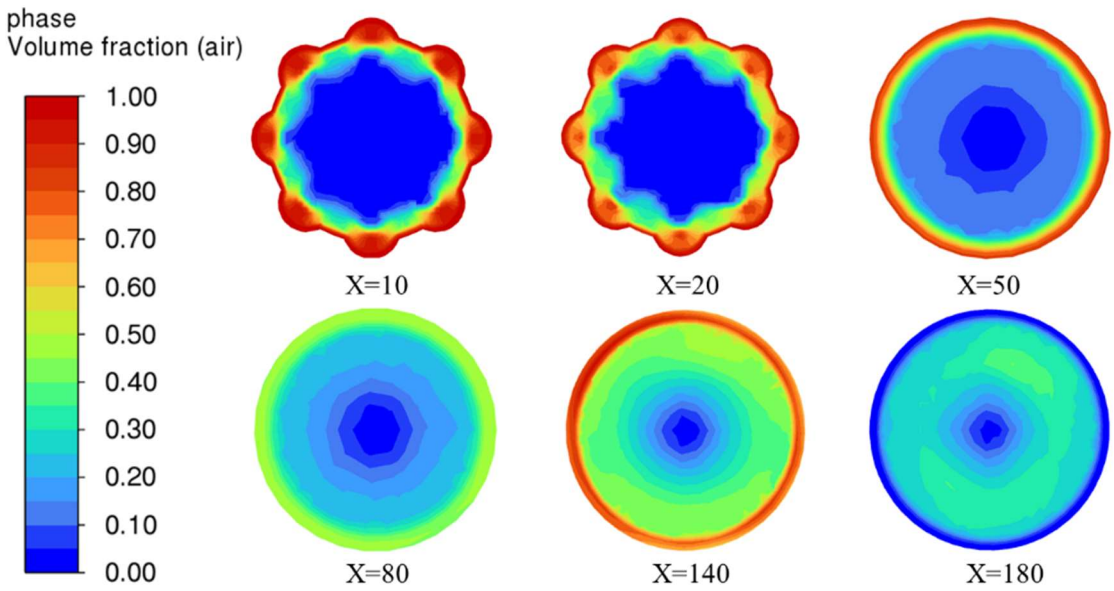

Figure 6. Radial distribution of the gas phase cloud picture
(X=10: Front section of the arc-shaped flow channel, X=20: Rear section of the arc-shaped flow channel, X=50: Front section of the stepped tube, X=80: Rear section of the stepped tube, X=140: Diffuser pipe, X=180: Extension tube)

4.3 Particle Size Distribution of the Microbubble Generator

From Figure 7, it can be seen that the gas is evenly distributed through the annular air orifice into the concave areas of the arc-shaped flow channel, effectively preventing direct contact with the high-speed jet, resulting in minimal changes in bubble size in this region. After entering the latter part of the arc-shaped flow channel, the gas impacts the end face of the stepped tube, causing the gas to rebound off the wall and come into contact with the high-speed jet, where it is torn into fine bubbles under shear forces. Since the pipe diameter changes little at both ends of the stepped tube and the flow velocity and pressure variations are not significant, the bubble diameter stabilizes at 0.68 mm.

As seen in Figure 5, as the fluid enters the latter part of the stepped tube, the local flow velocity decreases, and the pressure increases, causing bubbles near the wall to break, reducing their diameter to about 0.65 mm. This indicates that high-speed flow has a stabilizing effect on bubble morphology, while changes in pressure are the key factor in bubble breakup. After entering the diffuser pipe, the larger pressure gradient induces significant deformation and fragmentation of the bubbles, with 80% of the bubbles' diameters reduced to 0.59 mm. In the extension tube, the reduced flow velocity makes the bubbles prone to coalescence in the low-velocity region, with their diameter mainly maintained around 0.78 mm. Through numerical simulation analysis, the novel jet-type microbubble generator, by improving bubble eccentricity and enhancing gas-liquid mixing, reduces the initial 1 mm bubble size to 0.68 ± 0.12 mm, with an average reduction of approximately 32% in size and a more concentrated bubble size distribution range.

ISSN: 2414-1895 DOI: 10.6919/ICJE.202506_11(6).0041

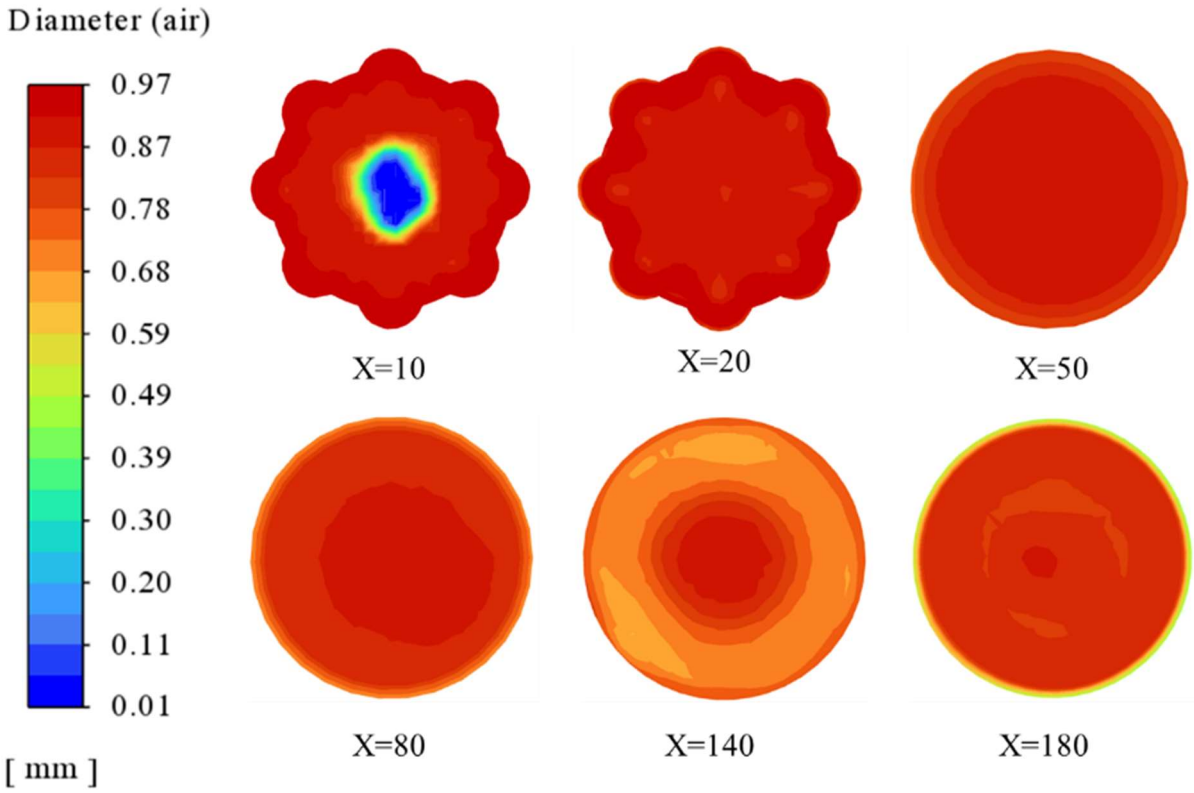

Figure 7. Bubble size distribution cloud map for each section

5. Structural Parameter Optimization Results Analysis

5.1 Effect of Annular Air Orifice Number on Microbubble Generator Performance

The number of annular air orifices is one of the key parameters for regulating the gas-liquid mixing efficiency and bubble generation characteristics in the BH-type microbubble generator. By setting the number of annular air orifices to 2, 4, 6, and 8 (corresponding to intake ratios R = 0.47, 0.93, 1.40, 1.86), the effects on axial pressure, average bubble diameter, and air intake were systematically studied.

As shown in Figure (a), the negative pressure intensity at the contraction tube significantly decreases with the increase in the number of orifices. When the number of orifices increases from 2 (R = 0.47) to 8 (R = 1.86), the pressure at the contraction tube rises from -16 kPa to -6.6 kPa, a decrease of about 59.3% in negative pressure intensity. This indicates that a higher intake ratio increases the dissipation of fluid kinetic energy. Theoretical analysis shows that the attenuation of negative pressure weakens the self-priming ability, but the actual intake increases linearly with the number of orifices. A quantitative comparison shows that expanding the intake area by 4.71 mm² improves intake efficiency by 114.6%, indicating that the gain from expanding the intake area dominates the increase in intake volume. The pressure in the arc-shaped flow channel stabilizes at -9 kPa, but when $R \geq 1.40$, the negative pressure increases to -10.1 kPa, which is closely related to the enhancement of shear due to turbulent energy in the early stage of gas-liquid mixing. The axial pressure curves in the downstream stepped tube and diffuser tube coincide with an overlap of 85%, indicating that changes in the number of air orifices mainly affect the neighboring flow field, with limited influence on the downstream disturbances.

ISSN: 2414-1895 DOI: 10.6919/ICJE.202506_11(6).0041

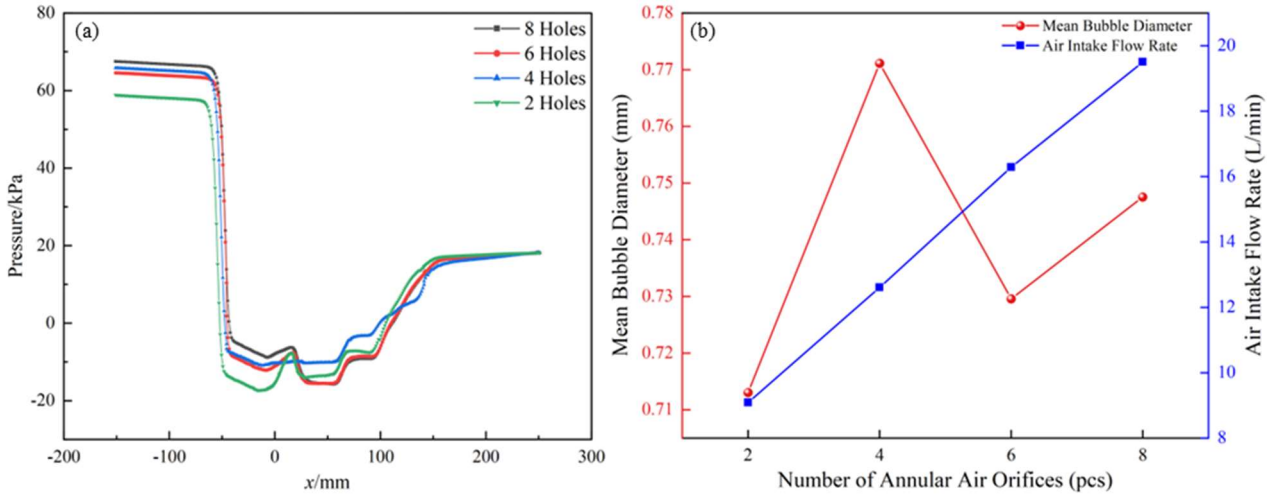

Figure 8. Effect of the number of annular air orifices on its performance:
(a) Axial pressure; (b) Average bubble diameter and air intake volume

As shown in Figure (b), the average bubble diameter at the diffuser tube outlet changes nonlinearly with the number of orifices. When the number of orifices is 4, the average bubble diameter reaches its maximum value of 0.771 mm, whereas it sharply decreases at 2 and 6 orifices. This phenomenon stems from a two-stage regulation mechanism: at low intake ratios, reducing the intake volume avoids bubble coalescence, making it easier for bubbles to break; at high intake ratios, the local pressure gradient significantly increases, leading to more intense bubble breakage and ultimately resulting in smaller bubble sizes. Therefore, considering the effect of the number of orifices on its performance, 6 orifices (R = 1.40) are chosen as the optimal structural parameter, as it ensures high intake volume and effectively reduces bubble size.

5.2 Effect of Diffuser Tube Angle on Microbubble Generator Performance

The diffuser tube is a key region for bubble breakage, and the appropriate angle directly affects bubble breakage and coalescence, thereby influencing the bubble generation characteristics of the microbubble generator. Numerical simulations were conducted for four diffuser tube angles: 3°, 3.5°, 4°, and 4.5°. The results are shown in Figure 9.

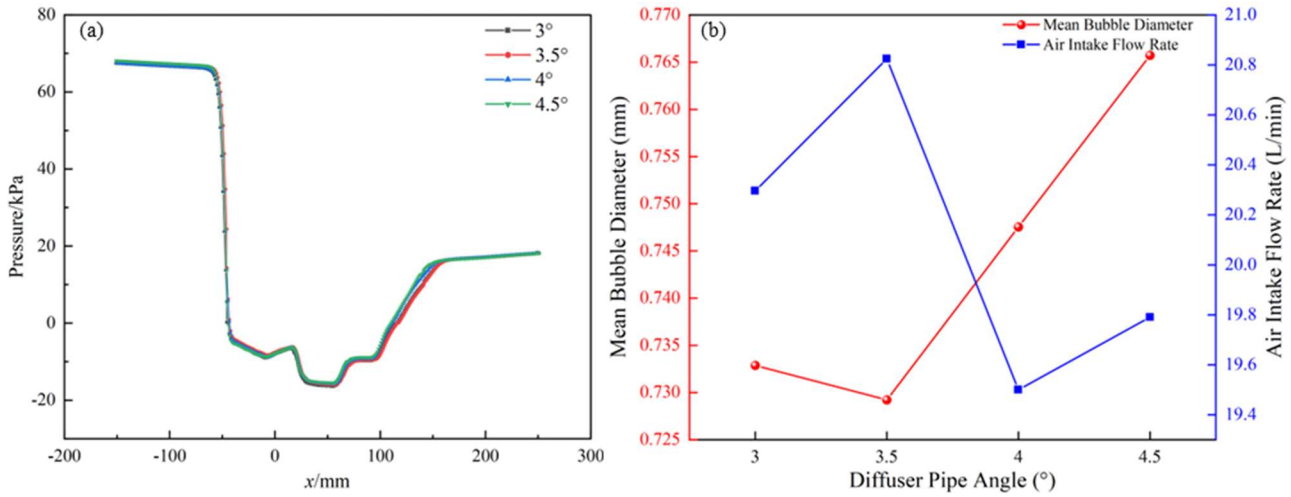

Figure 9. Effect of diffuser angle on performance
(a) Axial pressure; (b) Average bubble diameter and air intake volume

ISSN: 2414-1895 DOI: 10.6919/ICJE.202506_11(6).0041

As shown in Figure (a), the change in the stepped tube angle has little effect on the overall axial pressure distribution, with only slight variations at the diffuser tube. Additionally, the rate of pressure change increases as the angle increases. As shown in Figure (b), the intake volume fluctuates with the angle increase, but the overall change is small, only 1.4 L/min, indicating that the increase in the diffuser tube angle has a weak effect on intake volume regulation. The average bubble diameter decreases initially and then increases with the angle increase, reaching the smallest size at 3.5°. This phenomenon is caused by the following reason: as the diffuser tube angle increases, the local flow velocity decreases, and the bubble residence time is extended, resulting in the bubble breakage rate being lower than the coalescence rate, ultimately causing the bubble size to increase. A reasonable diffuser tube angle needs to balance the pressure gradient and flow velocity, enhancing bubble breakage while suppressing bubble coalescence, thus achieving smaller bubble sizes. Therefore, a diffuser tube angle of 3.5° is selected as the optimal structural parameter.

5.3 Effect of Stepped Tube Diameter Difference on Microbubble Generator Performance

This study replaces the traditional throat tube design with a stepped tube structure and selects diameter differences of -0.5 mm, 0 mm, 0.5 mm, and 1 mm for the front and rear of the stepped tube for simulation analysis. The effects of these diameter differences on axial pressure, average bubble diameter, and intake volume are systematically investigated.

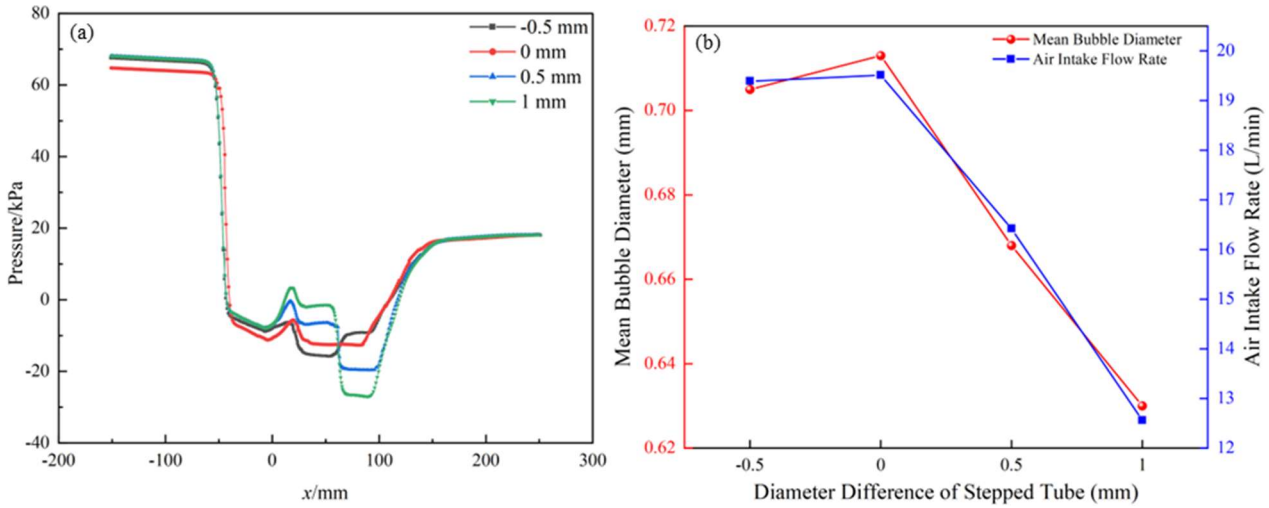

Figure 10. Effect of stepped tube diameter difference on performance
(a) Axial pressure; (b) Average bubble diameter and air intake volume

As shown in Figure (a), the diameter difference of the stepped tube has a significant impact on the axial pressure of the adjacent structures, with minimal impact at both ends of the device. In the front section of the stepped tube, the axial pressure increases as the diameter difference increases, with the maximum pressure difference reaching 8 kPa. In the rear section of the stepped tube, the axial pressure decreases as the diameter difference increases, with the maximum pressure difference reaching 17 kPa. This is due to the energy conversion caused by the changes in the tube diameter and the gas-liquid mixing, which in turn affects the axial pressure variation.

From the analysis of Figure (b), it can be observed that the increased pressure in the front section significantly weakens the negative pressure self-priming effect, reducing the intake volume. The pressure difference between the front and rear sections significantly decreases the bubble diameter

6. Conclusion

This study focuses on the structural innovation and parameter optimization of the jet-type microbubble generator to reduce bubble size and improve gas-liquid mixing efficiency, avoiding the

ISSN: 2414-1895 DOI: 10.6919/ICJE.202506_11(6).0041

gas eccentricity phenomenon caused by a single intake pipe. Based on CFD-PBM technology, the performance of the BH-type microbubble generator was analyzed, with a focus on the effects of the annular air orifice, diffuser pipe, and stepped tube parameters on bubble characteristics. The following conclusions were drawn:

(1) The design of the annular air orifice ensures that gas enters the pipe evenly from all directions, effectively preventing bubble eccentricity caused by single-side intake. This design improves the gas-liquid mixing efficiency to 45% and results in a more concentrated bubble size distribution.

(2) The design of the arc-shaped flow channel and stepped tube replaces the traditional throat, guiding the initial gas flow path and causing the gas to break into small bubbles before entering the stepped tube. This prevents large bubbles from entering the diffuser tube with high-speed jets, thus increasing bubble size and optimizing the flow characteristics in this region. At the same time, the acceleration effect of the stepped tube on the fluid effectively suppresses bubble coalescence.

(3) The results of the single-factor analysis show that bubble diameter is primarily affected by the intake volume and turbulent shear forces. The annular air orifice controls the intake volume by reducing the intake ratio RRR, inhibiting bubble size growth. The stepped tube and diffuser tube increase the flow velocity and pressure gradient, reducing the residence time for bubble coalescence and increasing the turbulent shear effect, which promotes bubble breakup. The intake volume is mainly influenced by the intake area and the negative pressure self-priming effect. By adjusting the intake ratio RRR, it is observed that, within a certain negative pressure range, the intake area is the primary factor affecting intake volume. Axial pressure changes are influenced by pipe diameter and gas content.

(4) Considering the practical application of the microbubble generator in engineering, bubble diameter is selected as the primary evaluation criterion, while intake volume serves as the secondary criterion. Therefore, the optimal structural parameter combination for the BH-type microbubble generator is 6 annular air orifices, a stepped tube diameter difference of 1 mm, and a diffuser tube angle of 3.5°.

References

[1] RAJAPAKSE N, ZARGAR M, SEN T, et al. Effects of influent physicochemical characteristics on air dissolution, bubble size and rise velocity in dissolved air flotation: a review[J]. Separation and Purification Technology, 2022, 289: 120772.

[2] TAO X H, LIU Y F, JIANG H, et al. Microbubble generation with shear flow on large-area membrane for fine particle flotation[J]. Chemical Engineering and Processing-Process Intensification, 2019, 145: 107671.

[3] ABADIE T, AWALI S M A, BRENNAN B, et al. Oxygen transfer of microbubble clouds in aqueous solutions-Application to wastewater[J]. Chemical Engineering Science, 2022, 257: 117693.

[4] LIU Q L, LIU S, LI Y D, et al. Microbubble-based process for the enhancement of microfine and heavy oil droplets swirl separation in axial inlet hydrocyclone[J]. Separation and Purification Technology, 2024, 332: 125642.

[5] ZhANG S J. Microinterfacial technology enhancing mass transfer in chemical engineering[J]. Green Energy & Environment, 2021, 6(4): 453-454.

[6] Li X Z, JIANG Z L, GUO Y L, et al. Research on the characteristics of a new microbubble generator based on the Venturi tube[J]. Chemical Engineering and Processing-Process Intensification, 2024, 203: 109876.

[7] LIU Yu. Measurement and numerical simulation of gas liquid two phase flow in Jet Micro-bubble generator[D]. Xuzhou: China University of Mining and Technology, 2018.

[8] ZHAO L, SUN L C, MO Z Y, et al. Effects of the divergent angle on bubble transportation in a rectangular Venturi channel and its performance in producing fine bubbles[J]. International Journal of Multiphase Flow, 2019, 114: 192-206.

ISSN: 2414-1895 DOI: 10.6919/ICJE.202506_11(6).0041

[9] BIE H Y, LI Y X, XUE L C, et al. A visualized investigation of bubble breakup in a swirl-venturi bubble generator[J]. Aiche Journal, 2023, 69(3): e17892.

[10] TANG Wencai, YAN Changqi, SUN Licheng, et al. Characteristic of bubble breakup in venturi-type bubble generator[J]. Atomic Energy Science and Technology, 2014, 48(05): 844-848.

[11] XU Y T, SHUAI Y, YANG Y, et al. Performance Evaluation and Scale-up of the Swirl-Venturi Microdroplet Generator[J]. Industrial & Engineering Chemistry Research, 2024, 63(18): 8416-8429.

[12] XU W G, LI W J, WANG J W, et al. Numerical Simulation of Gas-Liquid Two-Phase Flow CFD-PBM Model in a Micro-Nanobubble Generator[J]. Minerals, 2022, 12(10): 1270.

[13] CAO Junya, MA Mengjie, LI Pingping, et al. Effect of bubble intake direction on bubble diameters generated by a venturi microbubble generator[J]. Gold Science and Technology, 2017, 25(05): 127-134

[14] DING Guodong, CHEN Jiaqing, LI Zhenlin, et al. Analysis of the effect of air injection hole position on bubble formation characteristics of Venturi-type microbubble generator[J]. CIESC Journal, 2021, 72(11): 5552-5562+5437.

[15] WU Y X, CHEN H, SONG X F. Experimental and numerical study on the bubble dynamics and flow field of a swirl flow microbubble generator with baffle internals[J]. Chemical Engineering Science, 2022, 263: 118066.

[16] LIU Yuewei. Study on bubble size and mass transfer performance of new venturi bubble geneartors[D]. Beijing: Beijing University of Chemical Technology, 2023.